

This is the peer reviewed version of the following article:

Full-scale experiments of fire control and suppression in enclosed car parks: A comparison between sprinkler and water-mist systems / Santangelo, Paolo Emilio; Tarozi, Luca; Tartarini, Paolo. - In: FIRE TECHNOLOGY. - ISSN 0015-2684. - 52:5(2016), pp. 1369-1407. [10.1007/s10694-016-0569-3]

*Terms of use:*

The terms and conditions for the reuse of this version of the manuscript are specified in the publishing policy. For all terms of use and more information see the publisher's website.

11/01/2026 16:11

# **Full-Scale Experiments of Fire Control and Suppression in Enclosed Car Parks: A Comparison Between Sprinkler and Water-Mist Systems**

Paolo E. Santangelo <sup>a,b,\*</sup>, Luca Tarozzi <sup>c</sup>, Paolo Tartarini <sup>a</sup>

<sup>a</sup> *Dipartimento di Ingegneria “Enzo Ferrari”, Università degli Studi di Modena e Reggio Emilia,  
Via P. Vivarelli 10, 41125 Modena, Italy*

<sup>b</sup> *Department of Fire Protection Engineering, University of Maryland,  
3106 J.M. Patterson Building, College Park, MD 20742, USA*

<sup>c</sup> *Bettati Antincendio S.r.l., Via Disraeli 8, 42124 Reggio Emilia, Italy*

\* Corresponding author  
E-mail addresses: paoloemilio.santangelo@unimore.it, psantang@umd.edu  
Tel.: +39 059 205 6313  
Fax: +39 059 205 6126

# **Full-Scale Experiments of Fire Control and Suppression in Enclosed Car Parks: A Comparison Between Sprinkler and Water-Mist Systems**

## ***Abstract***

Recent efforts to investigate car-park fires and understand the related mechanisms have fostered the need for analyses of suppression performance against this type of fire scenario. This work aims at providing an insight into the ability of sprinklers and water-mist systems to control and extinguish a fire within an enclosed car park through a series of real-scale experiments. Three cars were employed in each test: the central one was ignited by a heptane pool fire and the adjacent ones served as targets. Two configurations were explored: in the first one, a nozzle was placed directly at the vertical axis of the ignition source, whereas the ignition source was located between the area coverage of four nozzles in the second one. The sprinkler system mainly served as a reference; two values of discharge density were evaluated for water mist at high operative pressure and a biodegradable surfactant was also tested against the most challenging configuration. A quantitative analysis of free-burn and discharge phases by temperature measurements was coupled with radiant heat-flux measurements and an assessment of post-fire damage. Sprinkler and water-mist systems were capable of containing the fire spread and thermally controlling the fire, thus preventing structural damage. The water mist's ability to overpower the plume and reach the burning surfaces proved more effective than that of sprinklers, especially as no nozzles were located right above the ignition surface. The higher discharge density showed better capability of preventing re-ignition phenomena and suppression was attained in both the investigated configurations, which suggests that a certain amount of flux is also needed to achieve flame cooling. The additive had promising impact on suppression performance; however, more tests are required to specifically explore its ability to enhance thermal control.

**Keywords:** car park; vehicles; suppression; thermal control; sprinkler; water mist

## 1. Introduction

Car parks have become a common feature of the built environment over the last 6 decades, as a direct consequence of the increasingly extensive presence of motor vehicles within urbanized areas. Several types can be identified: fully/partially enclosed or completely open; above ground or underground; single- or multi-storey; stand-alone buildings or attached to another – usually bigger – structure. Obviously, fire-safety problems associated with potentially large numbers of vehicles close to each other have arisen when designing car parks; some guidance to address these issues is provided in the technical literature, with specific reference to multi-storey buildings [1]. However, several fire events have occurred in this kind of facilities; among the most recent, it is worth mentioning the Gretzenbach, Switzerland incident (2004, underground park, 7 fatalities) [2], the Bristol, UK incident (2006, underground park, 1 fatality in the residential unit above) [2] and the Edinburgh, Scotland incident (2014, open car park at the airport, 18 destroyed cars) [3]. As an indicative number, more than 3000 car-park fires were reported in the UK over the 1994-2005 time span, more than a half of which started in a vehicle [2]. Therefore, a large interest in better understanding car-park fire phenomena has grown both in industry and in academia to ultimately develop suitable regulations and standards and possibly prevent or successfully face these events. Recently, this interest has increased in terms of available resources (e.g., the “Fire and Explosion Safety in Car Parks” project, funded by the Belgian IWT-Vlaanderen), awareness of the involved stakeholders at all levels [4] and scientific achievements [5].

Extensive research was performed by Chow and coworkers in the mid and late 90’s [6-10] on ambient conditions within enclosed car parks, which ultimately culminated in a comprehensive analysis that included fire. The first study [6] focused on identifying thermo-hygrometric conditions (temperature, air speed and relative humidity) associated with car-park users’ comfort, thus providing guidance to design both the structure and the ventilation system accordingly. The following works [7-9] were aimed at specifically understanding the relationship between carbon monoxide concentration and air flow parameters (air speed and turbulence intensity), which yielded to assess ventilation rate to contain carbon monoxide level. The use of computational fluid dynamics (CFD) was recommended to the purpose, yet being the proposed models validated against some experiments. As a connection with engineering practice, ventilation rate was ultimately discussed in relation with the number of vehicles within the car park and the aforementioned conditions for thermo-hygrometric comfort. Moreover, some mathematical modeling [9] allowed to estimate the reduction in

energy consumption through a two-level ventilation system, even more emphasized by the insertion of CO sensors. A self-developed CFD code was employed for ventilation assessment in [10] and the CFAST zone model was then used to simulate a potential fire case, thus adding some investigation of smoke control and sprinkler performance. This work suggests that some ventilation – either natural or mechanical – would be recommended even for the sole smoke extraction; the relationship between sprinkler activation and occupants' escape time was also explored, ultimately giving some guidance on the choice of sprinkler type. A recent study by Viegas [11] followed Chow's approach [10] to numerically evaluate the ability of impulse ventilation to contain the smoke flow from a fire event in an enclosed park. The interaction between the fire ceiling jet and the fan-driven flow was modeled to yield some criteria on size and displacement of the openings. Fire Dynamics Simulator (FDS) code was used by Zhang et al. [12] and Lin et al. [13] to investigate the effect of ventilation conditions on fire spread and smoke motion in large and complex car parks. They remark that ventilation tends to somewhat increase fire intensity, even though the limitations of CFD modeling of fire development as airflow is imposed still appear to be quantitatively addressed.

As a prominent example of coupled experimental and numerical approach, it is worth mentioning the long-term research carried out by the French CTICM (Centre Technique Industriel Construction Métallique) and partners on fire resistance of steel and concrete composite structures, typical of both closed [14,15] and open [16] car parks. Full-scale free burn tests were conducted on both single- and multiple-car fires; computational models were validated against those experiments and used to assess structural resistance. Whereas unprotected steel structure seems capable of withstanding a fire in an open car park [16], continuous beams and protected or composite columns are advised against multiple-car fires in closed parks [15], which may occur if no detection and suppression systems are provided.

An extensive use of CFD permeated the most recent research. Tilley et al. [17] performed a parametric numerical analysis on fires in enclosed car parks, ultimately extrapolating some relationships to calculate smoke-extraction velocity that would meet the allowed smoke-backlayering distance. Some remarkable outcomes were lately issued along the same line, as a result of both experimental [18,19] and numerical efforts [20]. Notably, Horváth et al. [18] performed both large- and reduced-scale experiments, showing the fidelity of these latter in reproducing smoke recirculation and accumulation mechanisms. Moreover, they predicted critical ventilation velocity at which no backlayering occurs through a typical road-tunnel model, even though applicable only to large car parks with mono-directional flow patterns.

Deckers et al. [19,20] carried out full-scale tests, then simulated by FDS. They found some relationships between smoke extraction rate and ceiling configurations, also emphasizing the code capabilities of properly reproducing turbulent air/smoke mixing phenomena. Other numerical studies were recently focused on car-park structural response to fires [21-24], effectiveness of design regulations against fire-safety criteria [25] and risk analysis [26].

As reviewed above, most recent research has been conducted on ventilation in enclosed car parks, also encompassing smoke control and extraction. Despite some prominent experimental works [2,14,15,18,19], a general prevalence of numerical studies is quite noticeable, even because of the considerable costs associated with fire experiments, especially those conducted on real-scale scenarios. Merci [5] and Merci and Shipp [27] stressed out the need for expanding fire-safety studies towards other directions, including suppression by water-based systems. The present work is aimed at responding to that demand, which identifies a current gap in the open scientific and technical literature, except for the tests conducted by Shipp et al. [2] on sprinkler performance. To this end, some full-scale experimental tests in enclosed car parks were carried out, employing both sprinkler and water-mist systems. The applicability of the latter is challenged by a comparison with the former in terms of thermal-control and suppression effectiveness, since only non-binding standard procedures developed by prevention bodies [28] are currently available to assess water-mist performance in this kind of scenario. Evaluating fire-control and suppression capabilities of water-based systems in a relatively small, real-scale, enclosed car park is the ultimate scope of this work. Its results may also serve as a reference for future numerical simulations of similar scenarios, where water discharge is included.

## **2. Experimental Facility**

Currently, there are a limited number of resources or guidelines to specifically evaluate the performance of a water-mist system against a fire scenario. Therefore, the tests presented in this work were generally set within the OH2 (Ordinary Hazard 2) class of the UNI EN 12845 standard [29] to preliminarily identify the dimension of the scenario. Along this line, some inspiration to devise an experimental facility came from the guidance in [28]. This document serves as a key source for testing sprinkler and water-mist systems in parking garages and many other hazardous scenarios. It also proposes a simple criterion to compare the performance of other water-based systems with that of a sprinkler one: nozzles – either sprinklers or others – shall have the same location within the test chamber and operate against the same fire conditions.

The test chamber was built within the prefabricated, large-scale facility at *TE.S.I. S.r.l.* (Anagni, Italy), which features corrugated steel walls. The chamber had base size of  $6.8 \times 11.6$  m (surface area of about  $79 \text{ m}^2$ ) and a 3.5 m height, since a secondary ceiling was positioned at that distance from the floor, as the facility height is 8 m. The main idea lying beneath these experiments was to challenge the suppression system by a fire ignited below a car, then assessing fire spread over that vehicle and possibly two other cars next to it. This setup is shown in Fig. 1; notably, two experimental configurations were explored varying the position of the ignition source with respect to nozzle location. The accelerant consisted of a typical heptane pool fire: two metal containers ( $600 \times 900 \times 100$  mm) were placed next to each other, under the central car and aligned with symmetry axes of the car base. Each container was filled with 14 l of water and 14 l of heptane. In the first configuration (C1, Fig. 1a), a nozzle was installed along the vertical axis of the 2-container assembly, at 0.22 m distance below the ceiling [29]; in the second configuration (C2, Fig. 1b), the heptane container was positioned in the middle of an area covered by 4 nozzles, all placed at the same height from the floor as in the first configuration. These configurations would allow investigating the impact of nozzle position with respect to the initial fire location in a car-park scenario. The location of the heptane pool was not varied with respect to the car, since Mangs and Keski-Rahkonen [30] observed very little impact of the ignition point on vehicle fire development, with specific reference to heat-release rate (HRR) trend.

A tilt-out opening is also part of the facility: this window is located on one of the vertical walls at the ceiling; it is  $6.8$  (shorter base dimension, Fig. 1)  $\times 0.8$  m (Fig. 2), which amounts to a surface area of  $5.4 \text{ m}^2$ . Since there was a gap of about 50 mm between the secondary ceiling and the walls (Fig. 2) – this evaluation of the gap takes the presence of the clamps into account – some space (approximately  $1.8 \text{ m}^2$  distributed along the secondary-ceiling perimeter) was available for air and gases to flow from the test chamber into the enclosed space above, then flowing out through the tilt-out opening (Fig. 2). Therefore, this setup is a case of naturally ventilated car park [2], even though the size of the vents was not imposed in accordance with any specific regulation. It is interesting to note that  $1.8 \text{ m}^2$  is smaller than  $1/20$  of the total floor area, as recommended for natural ventilation in [2], but is larger than  $0.06 \text{ m}^2$  per parking bay, which is the rule tested by CFD in [15] as required in some European countries. The vertical walls of the facility are not sealed to the floor, so air inflow was naturally allowed throughout each experiment.

As already mentioned, each test involved 3 cars, arranged in the chamber as shown in the sketches of Fig. 1 and in the photo of Fig. 3. All the employed vehicles were chosen to be of

similar size, combustible components (e.g., car mats, spare tire) and classification (e.g., sedan, station wagon). To this end, very similar models (*Rover 414i*, *Rover 214 Si*, *Citroën ZX 1.4i* and *Ford Sierra 2.0i*) – especially in size and curb weight (1140 – 1480 kg) – were used as the central car in the tests, thus ensuring high level of consistency against the core of the fire scenario; various models were employed as target vehicles throughout the experiments, which also obeyed to the aforementioned characteristics of similarity. All the employed cars were in running order. Mainly for safety reasons and to generally avoid explosion hazards, the following actions were taken on the vehicles before each test:

- all liquids (e.g., fuel, motor oil, brake and transmission fluids, coolants, lubricants) and pressurized gases (e.g., in the shock absorbers) were removed;
- airbags were removed;
- tires were fully deflated and chassis were held at their operative distance from the floor by suitable holders.

The effect of these conditions against the ability of the tests proposed in this work to reproduce actual car-park fires needs some discussion. Those cars can be generally considered as compact or medium, in accordance with the weight- and size-based classifications provided by Tohir and Spearpoint [31] in their review of fire characteristics of passenger vehicles. These classes represent 50 – 60% of the vehicle population overall [32]. An analysis of HRR throughout free burn of various models ranging from mini to heavy seems to suggest that the main variation lies in the peak value and the time to reach it, provided that the initial slope may considerably change even between models belonging to the same class [31]. The mean time to peak ranges from 15 to 38 min (excluding the case of a SUV model, which yielded a value of less than 4 min) after ignition; suppression systems are commonly expected to activate discharge well before those times, so successful suppression would actually imply some independence of the class of the involved vehicles. However, Shipp et al. [2] noticed the ability of sprinklers to contain a car-park fire even in their unsuccessful suppression cases, which might be somewhat related to the vehicle size.

The early experiments by Mangs and Keski-Rahkonen [30] suggest that gasoline in the tanks ignites between 20 and 30 min after ignition (local HRR peak), thus allowing to consider the absence of liquid fuel as not strictly significant in suppression tests. However, steel tanks were employed in [30]; Shipp et al. [2] chose to test plastic tanks, as more common in most recent cars. A cone-calorimetry test on tank flammability yielded to a critical heat flux of  $16.5 \text{ kW m}^{-2}$  and time to ignition between 290 and 300 s at  $20 \text{ kW m}^{-2}$



irradiance [2]. Those values may imply an earlier gasoline ignition than that mentioned in [30], thereby making the presence of liquid fuel a possible contribution to fire development. In fact, temperature measurements within the tank in [2] show readings lower than 100 °C until about 40 min after ignition, which suggests that actual irradiance to the tank was definitely lower than that tested in the cone calorimeter. As for other fuel types, Shipp et al. [2] claim that LPG- or hydrogen-fueled cars have not proven a particular danger in a car-park fire. Obviously, gas leakages (e.g., valve malfunctioning, cracks) may result in severe consequences, such as explosions [26]. The presence of other fluids is not reported as remarkable in the HRR trend, as well as pressurized air in tires [30]. Currently, no reference to airbags is made in the open literature; however, they may be subject to explosion, especially as flashover is reached in the passenger cabin. This event may occur about 10 min after ignition [2,30] and should be avoided by an earlier discharge activation.

### 3. Discharge Systems

As already remarked in Section 2, a reference sprinkler system was designed in accordance with standardized guidelines [28,29] and installed in the test chamber; almost the same spacing between nozzles was also employed in the experiments by Shipp et al. [2]. A water-mist system was then tested against the same fire scenario, provided that its nozzles had the same location within the domain as those of the reference one (Fig. 1). The area coverage of each nozzle results from the imposed spacing as equal to about 12 m<sup>2</sup>; being nozzle K factor a known parameter, discharge density was obtained by simply dividing the volume flow rate at the desired operative pressure by area coverage. An account of these quantities is presented in Table 1 as related to each test. Obviously, discharge density is a generic, single-value expression of water flux; a detailed characterization of the released sprays would imply measuring flux distribution at various locations over the coverage area, as suggested by Ren et al. [33] for sprinkler sprays and by Santangelo [34,35] and Santangelo et al. [36] for water mist. As mentioned in Section 2, the nozzle outlet was set at 0.22 m distance from the ceiling [29]. Steel pipes and an electric pump (maximum static head of 130 bar) were also inserted.

#### 3.1. Sprinkler

As reported in Table 1, the same value of discharge density was employed in the sprinkler tests (C1SPK and C2SPK); this condition was achieved by operating pendent sprinklers (Fig. 4a) at 1 bar. Those nozzles are manufactured by *CPF Industriale S.r.l.* under the code SKR 15; their outlet orifice  $d_o$  has a 15-mm diameter and the operation temperature is 68 °C. Chow

[10] applied the same threshold temperature for sprinkler thermal activation, yet using early-stage fast-response (ESFR) heads in the simulations, whereas the nozzles employed in the present study feature standard response.

Initial characteristic drop size was evaluated through the relationship found by Heskestad [37] between Volume Median Diameter  $d_m$  and droplet  $We$  number ( $\rho_w u^2 d_o / \gamma_{wa}$ ):

$$\frac{d_m}{d_o} = C We^{-1/3}, \quad (1)$$

where  $\rho_w$  is density of water ( $= 998.2 \text{ kg m}^{-3}$  at  $20^\circ\text{C}$ ),  $u$  is droplet initial velocity,  $\gamma_{wa}$  is surface tension at the water/air interface ( $= 7.2 \cdot 10^{-2} \text{ N m}^{-1}$  at  $25^\circ\text{C}$ ) and  $C$  is a constant. Droplet initial velocity was evaluated by a simple Bernoulli model ( $\sqrt{2\Delta p / \rho_w}$ ), where the pressure difference between inlet and outlet section  $\Delta p$  was considered as equal to operative pressure. Obviously, this assessment neglects friction losses through the nozzle and is based upon the assumption that static load is fully converted into dynamic load [34-36,38]. As for the  $C$  constant, the value (2.7) suggested by Lawson et al. [39] was used in this study, since it resulted from drop-size measurements conducted on sprinklers similar in orifice diameter (11 – 15 mm) and released flow rate ( $1 - 2 \text{ L s}^{-1}$ ). The  $d_m/d_o$  ratio turned out as 0.08, which reasonably agrees with the values found by Lawson et al. [39] for  $We$  numbers in the  $10^4$  order of magnitude, as in the present work. This calculation yielded to a Volume Median Diameter of about  $1170 \mu\text{m}$ .

### 3.2. Water Mist

Two water-mist nozzles were employed to achieve the values of discharge density for tests C1WM1.5, C1WM2.0, C2WM1.5, C2WM2.0 and C2WMA (Table 1). Those nozzles have the same geometry and belong to the same series manufactured by *Bettati Antincendio S.r.l.*: as shown in Fig. 4b, they feature a thermo-sensitive bulb at the bottom center and 6 injectors at the lateral, inclined surface. The operation temperature is  $68^\circ\text{C}$  – consistent with sprinklers (Sub-section 3.1) – and the discharge activates at super-fast response. Each injector is a pressure-swirl atomizer, where two tangential slots allow water to flow into the swirl chamber, then entering the convergent-divergent final duct. Their spray characteristics were studied by Santangelo [34,35] and Santangelo et al. [36] and they were employed against both canonical [40] and large-scale [41] fire configurations. In the present work, the lower discharge density was achieved by injectors having  $K$  factor of  $0.315 \text{ L min}^{-1} \text{ bar}^{-0.5}$  and orifice diameter of  $0.95 \text{ mm}$ ; as for the higher discharge density, the injector  $K$  factor was

0.410 L min<sup>-1</sup> bar<sup>-0.5</sup> and orifice diameter was 1.15 mm. Operative pressure was set at 91 and 95 bar respectively, so falling within the high-pressure water mist category (> 35 bar).

The calculation of characteristic drop size followed the inviscid-fluid approach to high-pressure sprays by Giffen and Muraszew [42,38], validated by Santangelo [35] for these water-mist atomizers. Notably, the discharge coefficient  $C_D$  is a function of air-core to total orifice area ratio  $X$ :

$$C_D = \left[ \frac{(1-X)^3}{1+X} \right]^{0.5}, \quad (2)$$

where the discharge coefficient is also a function of total orifice area  $A_o$  and flow number  $FN$  (the K factor, as typically indicated in fire-protection applications):

$$C_D = \frac{FN}{A_o} \left( \frac{\rho_w}{2} \right)^{0.5}. \quad (3)$$

Therefore, the discharge coefficient can be calculated from Eq. (3), thereby obtaining  $X$  from Eq. (2). The sheet thickness at the orifice  $t$  is a function of air-core to total orifice area ratio:  $d_o \cdot (1 - X^{0.5})/2$ ; as shown by Rizk and Lefebvre [43], Sauter Mean Diameter (SMD) presents a dependence on  $t^{0.39}$ . Santangelo [35] found that the  $SMD/t^{0.39}$  ratio is almost equal to 4 for water-mist pressure-swirl atomizers with orifice size between 0.49 and 1.14 mm, K factor between 0.117 and 0.417 L min<sup>-1</sup> bar<sup>-0.5</sup> and operating in the 50 – 100 bar range. Therefore, the SMD was calculated employing a 4.19 constant multiplier (the value obtained for conditions closer to those of the present study [35]) and resulted as equal to 34 and 36  $\mu$ m for the 0.95-mm and the 1.15-mm orifice respectively.

The use of additives to enhance suppression capabilities of water-based agents is gaining some popularity [41,44], even though their actual effectiveness against specific fire scenarios is still not completely understood [44]. Therefore, the applicability of a commercial surfactant to car-park fire cases was challenged in the present experiments. Notably, the Fire Seal produced by *BioEcoLogica S.r.l.* was chosen: it is constituted by anionic surfactants and is almost fully (~ 90%) biodegradable, a characteristic quite in-demand also for fire-protection chemicals. This additive is claimed to perform both an encapsulating (i.e., isolating the fuel surface [44]) and a gas-cooling action, together with making pollutants resulting from combustion convertible in water and CO<sub>2</sub> by bacteria. The recommended volume concentration of this surfactant is between 3% and 10%; the lower end of the range was applied here. Estimating the influence of additives on droplet size is generally quite difficult in the absence of dedicated experiments, as governing parameters like chemical components and concentration may imply a wide range of variability. The study by Stroup et al. [45]

presents a comprehensive performance assessment of degradable surfactants against various fire classes. Their tests on spray characterization show a variation of about  $\pm 15\%$  in characteristic droplet size with respect to sole water, as 4 additives are inserted under a concentration range of 1 – 3%. In particular, a 3% concentration seems to imply a decrease of 5 – 7% in Volume Median Diameter.

#### **4. Instrumentation and Approach to Data Analysis**

The test chamber was equipped with considerable diagnostics to evaluate fire development and suppression performance under a quantitative extent. As a typical approach to full-scale experiments [2,14,15,18,19,41], temperature trends at various locations were measured to assess the ability of the systems to thermally control and ultimately overpower the fire. Additionally, history of remarkable events and videos were recorded for each test; post-fire evaluations were conducted on the cars.

##### ***4.1. Diagnostics and Test Procedure***

A setup of 9 thermocouples was installed (Fig. 1) at 75 mm below the ceiling, since one the parameters to assess fire-control capability is ceiling-gas temperature as a reference for potential structural damage [46]. Suitable umbrella-like guards were added to each thermocouple to prevent it from being directly wetted by water droplets during system discharge. Obviously, recirculation due to either drag forces by fire plume or convective motions could imply some contact between smaller droplets and thermocouple beads. However, this phenomenon appears to be quite unlikely in such a large-scale compartment [41], where smaller droplets tend to rapidly evaporate as they move downwards.

As suggested by the guidelines for sprinkler tests against car-park fires [28], 3 plate thermometers were constructed and placed at 0.6 m distance from the car fronts and at 0.6 m from the floor (Figs. 1 and 3). These devices were developed and proposed by Ingason and Wickström [47] to evaluate radiant heat flux through a local temperature measurement within the exposed region. K-type thermocouples were employed; the related bias yields to a maximum systematic error of  $\pm 9\text{ }^{\circ}\text{C}$  in the operative range  $-200 - 1200\text{ }^{\circ}\text{C}$  ( $\pm 0.75\%$  according to standard IEC 584-2). The acquisition frequency was set as 1 reading per second.

In addition, water pressure was monitored at the outlet of the pump (P01, Fig. 1) and at the hydraulically most unfavorable nozzle (P02 in Fig. 1a and P03 in Fig. 1b). Supplied water flow rate was also measured (Fig. 1). The time of the following remarkable events was also recorded: ignition of the heptane pool fire (then considered as instant 0 of the timeline), first

discharge activation (first nozzle to activate), following discharge activations, flame extinction (if applicable and inferred from videos and temperature trends), end of the discharge.

The operative procedure consisted of lighting the heptane pool, then allowing free burn until the first nozzle activated upon rupture of its bulb. Thirty minutes of discharge were set as the operative time of the suppression system, being the water reservoir thereby sized in accordance with this imposed condition. However, emergency operations (i.e., entering the test chamber and manually extinguishing the fire) were possible throughout each test, in case any temperature reading at the ceiling reached 350 °C: this condition was applied to prevent structural damage to the facility [41] – especially to steel beams and columns [15,16,48] – even though it would have implied an early interruption of the test and an implicitly failed suppression.

Seven tests were conducted against the fire scenario described in Section 2, employing either sprinkler (reference) or water-mist nozzles described in Section 3. Table 1 reviews and summarizes the experimental settings of each test. As already reported, reference tests were carried out on both C1 and C2 configurations; the water-mist system with sole water was then operated against those configurations under 2 different discharge conditions (ultimately related to discharge density). One single test with a water/additive water-mist discharge was realized against configuration C2, since this was *a priori* considered the most challenging, as no nozzle was placed along the vertical axis of the ignition source.

#### **4.2. Evaluation Methods**

The evaluation of fire-control and suppression performance arose out of a methodology that accounts for various aspects, ranging from a post-fire investigation of the vehicles to an analysis of temperature readings. The procedure consisted of determining the following quantitative and qualitative parameters:

1. damage to the central car (i.e., tires, windscreen, side and rear windows, body and chassis, interiors) and fire development through it;
2. potential damage to the target cars (all the items mentioned at point 1);
3. temperature profiles, peak temperature values, average and maximum averaged values.

The analysis of points 1 and 2 was both qualitative and quantitative and largely inspired by Mangs' and Keski-Rahkonen's approach [30]. For instance, broken glasses were mainly evaluated under a YES/NO logic and possibly coupled with some observations, whereas

damage to other parts, such as tires, could be assessed more quantitatively by visually determining the amount of burned materials. As for point 3, some formulations of temperature average and maxima are proposed here as representative of a number of mechanisms. Obviously, a temperature matrix  $T_{ij}$  was collected for every test, where  $T$  is temperature, index  $i$  refers to a generic acquisition (and implicitly to time) and index  $j$  refers to a generic thermocouple (and implicitly to a spatial location almost at the ceiling height). Therefore, a peak temperature  $T_{peak}$  can be defined as the maximum value in the  $T_{ij}$  matrix; this parameter hints at the maximum thermal stress imposed by hot gases to the car-park structure. Along this line, an average peak temperature results from averaging maxima over the measurement locations:

$$T_{peak,ave} = \frac{\sum_j (\max(T_i))_j}{9}, \quad (4)$$

where  $(\max(T_i))_j$  is the maximum value over the whole acquisition time at the  $j$ th location. Since this formulation somewhat accounts for spatial temperature variation and fire spread, another expression is suggested to include spatial extent of the fire as the maximum value is reached at a certain location. If  $\tau_j$  is the time at which maximum temperature is read by the  $j$ th thermocouple, an average temperature at that time over all the sampling locations  $T_{max,ave,j}$  is yielded by:

$$T_{max,ave,j} = \frac{\sum_j T_{\tau_j j}}{9}. \quad (5)$$

Then, another average over all the 9 averaged temperatures calculated at each time at which a local maximum is reached is expressed by:

$$T_{max,ave} = \frac{\sum_j T_{max,ave,j}}{9} = \frac{\sum_j (\sum_j T_{\tau_j j})}{9 \cdot 9}. \quad (6)$$

$T_{peak}$  and the average maxima expressed by Eqs. (4) and (6) are single values and serve as concise indicators of the biggest extent reached by the fire in each test. However, some representation of fire evolution as a function of time is also meaningful. Thus, a peak-temperature trend  $T_{peak,i}$  can also be expressed as the maximum value over the 9 thermocouple readings at each acquisition time  $i$ . The same approach allows calculating a location-based average-temperature trend  $T_{ave,i}$  as the average value over the 9 thermocouple readings at each acquisition time  $i$ . As inspired by Yule [49] and Orlandini et al. [50], a simple 5-point moving average was also implemented to calculate the first derivative of  $T_{ave,i}$  with respect to time  $t$ ,  $\left(\frac{dT_{ave,i}}{dt}\right)$ . This quantity hints at the ability of the systems to thermally

control the fire; even though it does not unequivocally determine successful or unsuccessful suppression, it serves as a useful indicator of the various possible phases (e.g., fire growth, spray/flame interaction, potential suppression, re-ignition).

These parameters provide a representation of fire development through free burn and spray discharge. It is worth remarking that the parameters proposed in this sub-section were formulated to analyze the specific series of tests conducted in the present work, which features instrumentation and setup described in this section. However, both the methodology and the relationships may serve as a guidance to interpret results from full-scale tests equipped with similar diagnostics.

Finally, the dataset from plate thermometers was analyzed to possibly infer HRR from the car fires, at least until discharge was activated, since wetting of the exposed surface and the presence of water droplets between flames and plate may imply severe bias. To this end, a comparison was made with the test cases (i.e., pool fires) under known HRR proposed in [47]. This task mainly aimed at challenging both the standard guidelines [28] and hot-plate thermometry technique in capturing the order of magnitude of a car-fire size. Incident radiant heat flux onto the hot-plate thermometer was calculated by the following formula [47]:

$$\dot{q} = \frac{\varepsilon_{PT}\sigma T_{PT}^4 + (h_{PT} + K_{cond})(T_{PT} - T_{\infty}) + \rho_{st}c_{st}s(\Delta T_{PT}/\Delta t)}{\varepsilon_{PT}}, \quad (7)$$

where  $\dot{q}$  is heat flux,  $\varepsilon_{PT}$  is emissivity of the plate thermometer ( $= 0.95$ ),  $\sigma$  is the Stefan-Boltzmann constant ( $= 5.67 \cdot 10^{-8} \text{ W m}^{-2} \text{ }^{\circ}\text{C}^{-4}$ ),  $T_{PT}$  is the temperature reading of plate thermometer,  $h_{PT}$  is convective heat-transfer coefficient ( $= 10 \text{ W m}^{-2} \text{ }^{\circ}\text{C}^{-1}$  [47]),  $K_{cond}$  is conduction correction factor ( $= 22 \text{ W m}^{-2} \text{ }^{\circ}\text{C}^{-1}$  [47]),  $T_{\infty}$  is ambient temperature (initial thermocouple reading),  $\rho_{st}$  is steel density ( $= 8100 \text{ kg m}^{-3}$ ),  $c_{st}$  is steel specific heat capacity ( $= 400 \text{ J kg}^{-1} \text{ }^{\circ}\text{C}^{-1}$ ),  $s$  is steel plate thickness ( $= 0.7 \text{ mm}$ ) and  $t$  is time. Quantities like  $h_{PT}$  and  $K_{cond}$  were taken as equal to those used in [47], even though a more rigorous evaluation could challenge their general applicability, especially when considering convective heat transfer. However, the radiative heat transfer component should be the predominant mechanism in plate thermometry, thus limiting potential errors related to these assumptions.

## 5. Results and Discussion

The dataset resulting from the performed experiments was analyzed through a comparative perspective that not only aimed at assessing water-mist capabilities against those of sprinklers, but also focused on evaluating the performance of both systems against two fire configurations in the same scenario. That includes determining their ability to thermally

control and possibly suppress the fire, together with containing fire spread and limiting damage to central and target cars. Firstly, a summary of the experiments is presented to provide an account of settings and both initial and post-fire conditions for each test. Then, a quantitative analysis of thermal parameters and trends is introduced, together and in relation with nozzle activation times; finally, burning and damage to the vehicles are illustrated, highlighting the connection with fire evolution and spread. An assessment of experimental uncertainty and a discussion of applicability and limitations for the present study is also provided.

### ***5.1. Summary of Test Conditions and Post-Fire Evaluations***

As shown in Table 1, 3 tests were conducted on configuration C1, where a nozzle was placed at the vertical axis of the heptane tray (ignition source, Fig. 1a). Notably, one test was carried out employing the sprinkler heads introduced in Sub-section 3.1 at discharge density of  $6.5 \text{ L min}^{-1} \text{ m}^{-2}$  (test C1SPK), whereas 2 tests featured the water-mist nozzles discussed in Sub-section 3.2 at 2 values of discharge density:  $1.5 \text{ L min}^{-1} \text{ m}^{-2}$  for test C1WM1.5 and  $2.0 \text{ L min}^{-1} \text{ m}^{-2}$  for test C1WM2.0. The same values of discharge density were challenged for both sprinkler (test C2SPK) and water-mist (tests C2WM1.5 and C2WM2.0) systems against configuration C2, where the heptane tray (Fig. 1b) was positioned at the center of an area covered by 4 nozzles. An additional test was run on configuration C2 to explore the performance of a water/additive discharge (Sub-section 3.2), employing water-mist heads at  $1.5 \text{ L min}^{-1} \text{ m}^{-2}$  discharge density (test C2WMA). As a first and general observation, no emergency operations were required (Sub-section 4.1), so all the tests were terminated after a 30-min discharge. However, smoldering materials were still present at the end of each test, thus needing manual extinction. Therefore, extinction was technically not achieved [46] by either the sprinkler or the water-mist systems under the investigated conditions.

Table 2 presents an account of the post-test damage evaluation for all the experiments on configuration C1. In test C1SPK, it was quantitatively assessed that 4 tires of the central car were burnt and showed a 50% mass loss, whereas no glasses<sup>1</sup> were broken. However, the exterior exhibited severe burning, as shown by the comparison between Fig. 5a (pre-testing) and Fig. 5b (after-testing). The interior of the central car showed burn marks and evidence of materials loss, especially in the trunk (comparison between Fig. 6a and Fig. 6b); however, no

---

<sup>1</sup> In the present work, “glasses” refers to windows (i.e., windshield, side and rear windows) and does not include any other parts (e.g., headlamps, wing and rear-view mirrors). The vehicles employed in this study did not feature glass-panel roofs.



mass loss was quantified for the spare tire. The target cars appeared completely untouched and not involved by the fire. In tests C1WM1.5, one tire of the central car got fully burnt and 2 exhibited a 50% mass loss. Cracks were observed in one of its glasses and the exterior was generally as burnt as in tests C1SPK (Fig. 5b). The interior of the central car appeared to sustain almost the same damage as that in test C1SPK: some burn marks and materials loss mainly in the trunk (Fig. 7). The spare tire was not involved. Unlike test C1SPK, it was observed that one fender of Target 1 car was mildly burnt (rear fender in Fig. 8a), as much as the lateral plastic bar of Target 2 car (Fig. 8b). As for test C1WM2.0, 2 tires of the central car were fully burnt and 2 lost 50% of their mass; no glasses showed any damage. The exterior exhibited severe burning as in tests C1SPK and C1WM1.5, whereas the interior showed burn marks, but no evidence of materials loss, even for the spare tire. Generally, the target cars did not appear involved in the fire; however, Target 2 car was mildly blackened on the side facing the central car (Fig. 8c).

The evaluation of post-test damage for all the experiments on configuration C2 is shown in Table 3. One tire of the central car in test C2SPK was completely burnt and the other 3 sustained a 50% mass loss; no glasses were broken and the exterior appeared severely burnt as in tests C1SPK (Fig. 5b). While the spare tire was not involved with fire, the interior burnt more than that of central car in test C1SPK and materials loss of plastic parts occurred even in the front seats and dashboard (Fig. 9). The target cars were not involved in the fire. In test C2WM1.5, one tire of the central car was fully burnt and 2 underwent a 50% burning. No glasses sustained any damage and the exterior generally appeared severely burnt, as in test C2SPK. The interior showed burn marks, but no evidence of materials loss and the spare tire was not damaged. The target cars were not involved in the fire, but Target 2 car was mildly blackened on the side exposed to the fire of the central car, as in test C1WM2.0 (Fig. 8c). In test C2WM2.0, the central car had no damage to its tires, while one of the glasses showed some cracks. The exterior was severely burnt as in test C2SPK; in spite of no burning of the spare tire, evidence of mass loss in plastic parts appeared almost everywhere in the interior (comparison between Fig. 10a and Fig. 10b) and the damage was larger than those to the central car in test C2SPK (Fig. 9). No involvement in the fire was observed for the target cars. In test C2WMA, 2 tires of the central car sustained a 50% mass loss and 4 glasses were broken. The exterior underwent very severe burning and was more damaged than that of the central car in every other test. Figure 11a presents the pre-test conditions and Fig. 11b shows the car after testing; a comparison with Fig. 5b demonstrates the higher extent of burning in test C2WMA. The interior of the central car was severely burnt (Fig. 12), with materials

losses higher than any other test (Figs. 6, 7, 9 and 10) and widespread; notably, the spare tire was burnt (Fig. 12b), unlike any other test. The target cars did not show any sign of involvement in the fire.

## ***5.2. Temperature and Radiant Heat Flux***

Some temperature trends are proposed in Figs. 13 (configuration C1) and 13 (configuration C2), where initial ambient temperature was conveniently subtracted and time-coordinate origin was set at the first nozzle activation for each test. Initial ambient temperature ranged from 7 to 14 °C over the whole test series. The temperature history from TC5 (Figs. 13a and 14a) shows that configuration C2 was generally more challenging for the employed suppression systems, due to the absence of a nozzle right above the central car. Obviously, a sudden temperature drop at that location occurred as the first nozzle – N1, right above the ignition source – started discharging in configuration C1 (Fig. 1a, Table 4), whereas the first activated nozzle in configuration C2 – N8 (Fig. 1b, Table 5) – did not provide an immediate action against the fire occurring in the central car. In fact, the temperature trend of the C2WM1.5 case even shows a growth upon first activation. The average and peak temperature trends (Figs. 13b and 14b) for sprinkler system in configuration C1 (C1SPK) and all the cases of configuration C2 appear qualitatively more similar: even though the fire appears to be immediately overpowered in correspondence of the TC5 location, its spread over a wider area occurs for about 300 s, after which thermal control is achieved. The action of water-mist sprays right against the area of the ignition source (configuration C1) seems to favor a quick, if not sudden, overpowering of the flames all over the involved area. This observation can be physically explained by the ability of a high-pressure spray to overcome the flame and plume momentum, as found by Santangelo et al. [51]. However, it is interesting to note that re-ignition clearly occurred in the water-mist case with the lower discharge density in configuration C1 (C1WM1.5) at about 840 s; moreover, that case was characterized by 5 activated nozzles (Table 4), whereas 4 nozzles operated with the higher discharge density (C1WM2.0) and 3 in the sprinkler case (C1SPK). This difference can be arguably explained by the discharge density, which is an expression of water flux and ultimately connected with convective flame cooling [51]. Notably, cooling hot gases implies activating more water-mist nozzles in configuration C1, thus increasing the whole amount of released water and making it closer to that by sprinklers. That occurs in spite of a quicker overpowering of the fire plume by water mist. A possible re-ignition also happened in the sprinkler case (C1SPK) at about 400 s (100 s after the last nozzle activation). Re-ignition phenomena hint at the fact that

proper suppression was technically not reached [46]. Moreover, assuming that temperature trends – especially average temperature in Fig. 13b – are somewhat representative of HRR trend, only the water-mist case with the higher discharge density (C1WM2.0) shows a sharp reduction in configuration C1. Therefore, it can be conservatively stated that fire control was successfully attained in all the cases, whereas only the higher water-mist discharge yielded to suppression [46].

As for configuration C2, the same number of nozzles (4, Table 5) was activated by sprinkler and water-mist systems. That seems to strengthen the previous observations about spray/flame momentum competition: in a configuration where no nozzle is placed directly above the ignition source, that penalizes sprinklers even more. Although the discharge threshold between successful and unsuccessful performance could not be evaluated in the present study, it appears that sprinkler sprays may require higher fluxes to reduce the fire size by gas cooling than high-pressure ones (water mist), which mostly rely on penetrating the flames and reaching the hot surfaces [51]. Considering the water-mist trends for configuration C2 (Fig. 14b), the steep temperature decay at about 300 s suggests that the fire was overpowered, even at the lower discharge densities (C2WM1.5 and C2WMA). However, as in configuration C1, the lower water-mist discharge density with sole water (C2WM1.5) is characterized by an average-temperature reduction slower than that occurring for the higher density (C2WM2.0) or the water/additive case (C2WMA), once the fire is ultimately overcome (generally between 200 and 300 s after first nozzle activation, Fig. 14b). The sprinkler curve presents an even milder slope throughout discharge and evidence of re-ignition at 600 s (Figs. 14a and 14b), which somewhat resembles and even emphasizes the sprinkler behavior in configuration C1 (Fig. 13b). As on configuration C1, these observations allow claiming that both systems were capable of controlling the fire [46], but suppression was achieved only by the higher water-mist discharge density and by the water/additive discharge. When comparing water-mist performance under various conditions, the use of a surfactant appears beneficial in potentially leading to suppression even at a lower discharge density. However, more testing of water/additive action would be required to generally evaluate performance enhancement.

A combined analysis of nozzle activation times (Table 4 and Table 5) and first derivative of average temperature (Fig. 15) provides some additional assessment and insight into suppression performance. First of all, the initial car-fire development appears to have a certain degree of variability, as shown by the trends of Fig. 15 until first nozzle activation. This observation is consistent with the review of HRR curves of car free burns by Tohir and

Spearpoint [31] and explains the different first-activation times; moreover, it also justifies the initially higher temperatures reached in the water/additive test on configuration C2 (C2WMA) and presented in Fig. 14. In general, the fire growth seems faster in the tests of configuration C2, except for test C2WM2.0, thus explaining generally shorter first-activation times than in configuration C1. However, some variations arose even between tests under the same configuration. For instance, nozzle N1 activated slightly earlier in test C1SPK than in test C1WM1.5, even though super-fast response heads were used in water-mist tests (Subsection 3.2). This counterintuitive observation could be explained by the slightly milder temperature growth in test C1WM1.5 (Fig. 15b) than in test C1SPK (Fig. 15a), also perceivable from TC5-curve initial slope (from ignition to time 0) in Fig. 13a.

Figures 15a and 15d suggest a relatively similar behavior of the sprinkler system in thermally controlling the fire between the two configurations within a 600-s time span from first activation. Obviously, burning was more intense in configuration C2 and a higher amount of water was then discharged. Evidence of re-ignition is also shown for both configuration C1 at about 400 s (Fig. 15a) and configuration C2 at about 600 s (Fig. 15d), as previously noted about Figs. 13b, 14a and 14b. Figures 15b, 15c, 15e, 15f and 15g also support the same observation for the water-mist system, which was capable of achieving thermal control in about 300 s, even though a re-ignition phenomena occurred for the lower discharge density in configuration C1 (C1WM1.5) and triggered the activation of an additional nozzle. However, it is important to clarify that this relatively similar performance of the systems over the two configurations does not imply an independence of that, since, for instance, the maximum discharge occurred after shorter times in configuration C2 and less sprinklers were activated in configuration C1 (C1SPK). It is interesting to note that nozzles N1 and N5 were activated in all tests on configuration C1 (Table 4). The same nozzles – as expected, all those around the central car – in the same order (Table 5) were activated in all tests on configuration C2. However, it is also worth mentioning that 3 nozzles (N8, N9 and N10) started discharging at the same time at the lower discharge density (C2WM1.5 and C2WMA), thus suggesting the need for augmenting water flux, even in apparently momentum-driven suppression actions.

Figure 16 presents a comparison between suppression systems over the two configurations in terms of single-value parameters  $T_{peak}$ ,  $T_{peak,ave}$  from Eq. (4) and  $T_{max,ave}$  from Eq. (6). An average initial temperature was calculated for each test over the 9 thermocouples and subtracted to each of those quantities. The ability of both systems to control the fire and preserve structural integrity [46] is shown by peak temperatures: even in

the least favorable configuration (C2), this value is well below 300 °C, conservatively matching the guidance by Haremza et al. [48]. Shipp et al. [2] also showed sprinkler capability of limiting thermal stresses to the structure, even in cases where the fire was not put out. In general, temperatures were higher in configuration C2: that is largely due to the nozzle location and appears mostly unrelated to the variability in the free-burn phase, since peak temperatures were reached during discharge. However, a steeper temperature increase during free burn in the water/additive case (C2WMA) could explain a relatively higher peak temperature. The average peak temperature  $T_{peak,ave}$  and average maximum temperature  $T_{max,ave}$  hint at the fire spread and at the ability of the systems to contain it. This objective was achieved by both sprinkler and water-mist systems; mild differences arise out of a comparison on configuration C1 (Fig. 16): the higher discharge density (C1WM2.0) presents the lower values, thus supporting the need for effectively achieving flame cooling, together with overpowering the plume. Even though successful in thermally controlling the environment, the sprinkler system features higher average values with respect to water mist, thus emphasizing the already mentioned challenges for sprinklers as no nozzle is placed right above the ignition source. Even though using an additive seems to allow achieving suppression with lower discharge densities – as previously noted about the trends in Fig. 14b – it is also clear that the temperatures reached in test C2WMA were generally higher than those in the other tests on the same configuration (Fig. 14 and 16) from ignition through effective overpowering of the flames. That is partly justified by the variability of the free-burn phase (Fig. 15), which certainly proved more intense for test C2WMA; however, it is not clear whether the improvements by surfactants in terms of suppression effectiveness are combined with improvements in thermal control before drastically reducing the fire size. On the other hand, higher discharge densities (tests C1WM2.0 and C2WM2.0) seem to achieve both the objectives by flame penetration and flame cooling [51].

As already mentioned in Section 2, HRR trends of car free burn are available in the literature [2,30,31,52,53], as well as HRR and heat-flux trends from heat-flux meters for fire tests in car parks endowed with sprinkler systems [2]. An analysis of these works allows estimating that an early discharge activation (< 5 min) – as in all the experiments conducted for this study – faces a fire size in the range of 0.5-3 MW. Plate thermometry was employed as recommended by some guidelines [28] to evaluate incident radiant heat flux and possibly assess fire size. Calculated trends from temperature readings of plate thermometer PT1 (in front of the central car) are presented in Fig. 17 for each test over the free-burn phase; the

storage heat rate ( $\rho_{st}c_{st}s\frac{\Delta T_{PT}}{\Delta t}$ ) was not considered in these trends to smoothen the curves, as suggested by Ingason and Wickström [47] for measurements of fast temperature changes. In general, those profiles appear to well represent the fire growth and also to qualitatively support the already discussed observations about a certain variability in the fire development (Fig. 15). From a quantitative standpoint, the order of the evaluated incident heat flux is overall consistent with measurements obtained by heat-flux gauges [2] and with free-burn measurements (paper cartons), where plate thermometers were placed at almost the same distance from the fire [54]. Notably, a heat-flux meter at approximately 1-m distance from the ignited-car front recorded a slow increase from 0 to about 1 kW m<sup>-2</sup> as HRR – evaluated by a calorimeter – grew more rapidly up to about 2 MW, then remaining almost constant during the full involvement of that vehicle [2]. However, the values measured in the present study seem to be somewhat lower than expected in some tests (e.g., C2WMA) and some step-like increases (e.g., C1WM1.5) may or may not result from an actual, physical phenomenon. Notably, the flame development in a car fire may not be spatially homogeneous, especially in the transient phase before the car is fully engulfed. Moreover, if discharge occurs very early as in test C2WMA, the initial transient response of the instrument may not allow capturing the initial fire growth [2,47,54]. This technique was validated for canonical fire scenarios (e.g., pool and spray fires [47]) with steady fire size; its application to car-park fire cases appears promising, yet arguably requiring a higher number of plate thermometers around the vehicles and at various heights from the floor.

### ***5.3. Fire Damage to the Vehicles and Comparisons***

An assessment of fire damage to the cars is presented in Table 2 and Table 3 for configuration C1 and C2 respectively and a description is provided in Sub-section 5.1. As already remarked in Sub-section 5.2, the sprinkler and the water-mist systems proved capable of containing the fire spread in both the configurations: the central car generally underwent severe burning, yet being the target cars barely involved, if not completely untouched (Sub-section 5.1). It is also worth noticing that the fire in the central car did not reach a deep-seated stage in most tests, arguably all tests but C2WMA. However, some differences arise out of a comparison between tests. As expected, configuration C2 yielded to a more intense and longer burning of the central car, which resulted in damage not only to the exterior, but also to the interior. This is particularly evident for the sprinkler cases: the exterior got severely burnt (the photos of Fig. 5 serve as an example, even to compare pre-test and post-test

conditions) in both configurations, but tires and interior showed more damage in configuration C2 (Tables 2 and 3, Fig. 9). Differences in damage to the central car become less significant for the water-mist cases with sole water: the lower discharge density performed almost the same way against both configurations and the same considerations generally hold for the higher one, despite the fire spread quite noticeably within the interior in configuration C2.

Interestingly, the fire spread over the exterior of central cars tended to occur more from the center to the front in configuration C1 (e.g., Fig. 5b), whereas it appeared to be more uniform in configuration C2, with no preferential direction. This somewhat explains the order of nozzle activations in configuration C1 (Table 4 and Fig. 1a), since nozzle N1 was the first and nozzle N2 was the second for tests C1SPK and C1WM1.5. However, nozzle N2 did not activate in test C1WM2.0, arguably because of an already discussed (Sub-section 5.2) more effective and quicker action of the discharge, which ultimately led to suppression. On the other hand, the order of nozzle activation in all tests on configuration C2 (N8 – N9 – N10 – N11, Table 5, Fig. 1b) is probably also related to smoke motion and stratification, since no nozzle was placed right above the ignition source.

As already observed in Sub-section 5.2, the water/additive case (C2WMA) was characterized by remarkably more intense burning of the central car: a comparison between Fig. 12b and Fig. 5b gives evidence to the higher extent of damage, together with the account of destroyed glasses and spare tire – only case among all the tests – in Table 3. As already mentioned with regard to Figs. 14b and 15g, the fire developed more quickly in its free-burn phase, but it remains unclear from these experiments whether the presence of the additive is able to limit damage to the central car more than sole water.

As for target cars, the sprinkler system was capable of keeping them unburnt in both configurations, whereas some minor damage occurred with water mist. Notably, the water-mist test at the lower discharge density in configuration C1 (C1WM1.5) denoted some burning of the plastic parts in both the target cars (i.e., a fender in Fig. 8a and the lateral bar in Fig. 8b), whereas they were left almost untouched as the higher discharge density was applied (Sub-section 5.1, Table 2). The mild blackening of the target-car side exposed to the fire in tests C1WM2.0 (Fig. 8c) and C2WM1.5 likely resulted from flames being spread radially outwards as the heptane-pool fire was reached by a high-pressure spray [51] and lightly brushing against the target-car surface. However, the burnt plastic parts in test C1WM1.5 allow concluding that heat flux from the central-car fire reached the critical value for that material at that distance [2]. These observations suggest that configuration C2 was

less challenging from a fire-spread standpoint (Sub-section 5.1, Table 3), since the nozzle location provided a discharge onto the target cars; moreover, they strengthen the importance of releasing a certain amount of flux to achieve convective flame cooling, even when the fire plume is overpowered through momentum competition.

#### ***5.4. Experimental Uncertainty and Limitations of Full-Scale Tests***

As a brief note on experimental uncertainty, evaluating repeatability and reproducibility is quite difficult in tests at such a large scale. Moreover and as shown by profiles of Figs. 13-15, some variability in the car fire free-burn phase [31] must be taken into account. However, the degree of qualitative consistency in the overall free-burn behavior between tests supports the use of a similar approach to challenge suppression systems against car-park fires. Similarly, some discussion is ought about the limitations of the tests here presented, which are inherently characteristic of large-scale experiments. For instance, the major focus of this work is to challenge two fire-protection systems (sprinkler and water mist) having the same nozzle arrangement within the fire scenario and acting against two possible configurations. However, none of the systems failed to control and reduce the fire in any of the tests, thereby not allowing to highlight a threshold between unsuccessful and successful action. Such a threshold is usually proposed as a function of discharge – either in terms of critical flux or flow rate – and was achieved in previous studies on sprinklers and water mist against canonical liquid- [55,56], gas- [56] and solid-fueled fires [51]. Obviously, the scale of those works allowed identifying that threshold by varying discharge pressure through a series of experiments.

Numerous other variables were kept at fixed-value in the tests here presented; among the most significant, it is worth mentioning the distance between the nozzle outlets and the fire source, mainly related to ceiling height, and the distance between cars. The former stands as a longstanding question in suppression studies, since it impacts on the height at which the spray starts interacting with flames. However, few works present a parametric analysis with respect to that, even against canonical scenarios [56]. It is quite difficult to draw any conclusions about the effect of ceiling height on sprinkler or water-mist performance against car-park fires, since the only available terms of comparison are the experiments by Shipp et al. [2], where that parameter was set as quite close to the value used in the present work ( $\sim 3$  m). As for distance between cars, its variation obviously implies a different degree of fire spread from the ignited vehicle to the others, mainly by irradiation [2]. However, the present setup can be considered as conservative, since it focuses on cars occupying parking bays next to



each other. Moreover, the distance between adjacent cars (0.6 m) is slightly lower than the mean parking distance ( $\sim 0.7$  m) resulting from the survey over 18 car parks presented in [15].

Finally, the impact of ventilation on the results also needs to be addressed as a major question in spray performance within enclosed spaces. This issue is particularly important for water-mist systems, primarily because of smaller drop sizes: tiny, low-momentum droplets may be dragged away by ventilation-induced convective motions and fail to interact with the fire or its surroundings. As mentioned in Section 2, the present tests featured natural ventilation, somewhat consistent with previous works [2,15], yet not designed according to specific standards. Liu et al. [57] conducted an experimental study on the performance of two water-mist nozzles against canonical fires (e.g., pool and spray fires, wood-crib fires) in large compartments under various ventilation conditions (no ventilation, natural and forced ventilation). Notably, they tested a single-fluid nozzles discharging  $6 \text{ L min}^{-1}$  at 70 bar ( $D_{v90}$  between 200 and 400  $\mu\text{m}$ ) in a  $9.7 \times 4.9 \times 2.9$  m room, against fires between 0.5 and 0.7 MW. Those conditions are reasonably similar to the ones of this work, even though droplets were probably slightly larger and the fire size was comparable to the lower end of possible range of car fires as discharge started (0.5-3 MW, Sub-section 5.2). The room in [57] had a  $2.0 \times 0.9$  m door, which is equivalent to the area of the open space along the secondary ceiling (Section 2), yet being the orientation of the 2 surfaces different. Liu et al. [57] found no difference in suppression effectiveness between the no-ventilation (closed door) and the natural-ventilation (open door) cases, provided that the fire did not occur near the door. This outcome is attributed to the strong mixing between hot gases and high-momentum spray, which gets barely affected by opening a vent. Obviously, higher operative pressure like those employed in the present work would emphasize this phenomenon. Based upon the conclusions from [57], it can be assumed that natural ventilation in the present setup did not impact on water-mist performance, because the fire was initiated relatively far from the vents (Fig. 1) and did not appear to spread remarkably towards areas closer to them. However, a different positioning of the cars (e.g., very close to the walls) may have led to some significant effect of ventilation on the mist spray.

## 6. Conclusions

A series of full-scale experimental tests was conducted to assess fire-control and suppression [46] capabilities – including the ability to limit fire spread – of sprinkler and water-mist

systems against an enclosed, naturally ventilated car-park fire scenario. As inspired by some standards [28,29], two configurations were devised: a nozzle was placed at the vertical axis of the ignition source (central car) in the first one (C1), whereas the ignition source was located between coverage areas of four nozzles in the second one (C2). Sprinklers and water-mist nozzles had the same nozzle locations within the test chamber; one discharge density for sprinklers ( $6.5 \text{ L min}^{-1} \text{ m}^{-2}$ ) was compared to two for water mist ( $1.5$  and  $2.0 \text{ L min}^{-1} \text{ m}^{-2}$ ), these latter achieved at high discharge pressure ( $\sim 100 \text{ bar}$ ). Moreover, a biodegradable surfactant was added at low volumetric concentration (3%) to water mist under the lower discharge density in one test against configuration C2. Nozzles were thermally activated; temperature history was recorded over various locations at ceiling height; radiant heat flux was measured by hot-plate thermometers [47] and post-fire damage evaluation was conducted on the involved vehicles.

The sprinkler and the water-mist system were capable of controlling the fire in both the investigated configurations, without reaching any conditions potentially hazardous for the car-park structure. The fire never reached deep-seated stage prior to discharge activation, probably except for the mist/additive test and in the first instance both the systems proved able to extinguish the heptane-tray fire underneath the central car, which was used as the accelerant. As expected, the fire was more easily overpowered in configuration C1, whereas its spread to target cars was almost completely prevented in configuration C2, yet being very limited in configuration C1 as well. Re-ignition occurred in sprinkler and water-mist experiments at the lower discharge density; assuming that average-temperature trend at the ceiling height is representative of HRR trend, it can be conservatively concluded that suppression was achieved only by water mist at the higher discharge density on both configurations. High momentum and higher flux appear to combine penetration through hot gases to reach the hot surfaces and the need for achieving flame cooling, thus explaining a more effective performance of the higher water-mist density. However, the use of surfactants proved effective in suppressing the fire in configuration C2 even at the lower discharge density, yet being still unclear whether the employed additive led to improving thermal control prior to ultimately overpowering the flames. More tests are required to explore the actual enhancements by surfactants against this fire scenario.

Both free-burn phase and radiant heat-flux trends showed a certain variability in the fire development, which appears to be inherently characteristic of car fires [2,30,31]. Moreover, the absence of tests where successful fire control was not achieved does not allow to propose a critical threshold in terms of discharge density for both the systems against the tested fire

scenarios. The openings allowing natural ventilation do not appear to have an impact on fire-control and suppression performance of both systems, even though that may also be due to the positioning of the cars – relatively far from the vents – and the location where fire was initiated.

### Acknowledgements

The authors wish to gratefully acknowledge Mr. M. Bettati and Mr. F. Dignatici for their technical advising and helpful suggestions. This work was supported by the joint action of Bettati Antincendio S.r.l. (Italy) and Regione Emilia-Romagna (Italy) under the PRRIITT program.

### References

- [1] Hill J (2005) Car park designers' handbook. Thomas Telford Publishing, London, UK
- [2] Shipp M, Fraser-Mitchell J, Chitty R, Cullinan R, Crowder D, Clark P (2009) Fire spread in car parks. Final research report BD 2552. Building Research Establishment, Watford, UK
- [3] K. Richardson (2014) Electrical fault caused airport car park blaze. Edinburgh Evening News, 26 April 2014. Johnston Press, London, UK
- [4] Eurofeu Sprinkler Section (2009) Position paper on the fire protection of car parks. Eurofeu Sprinkler Section, Würzburg, Germany
- [5] Merci B (2013) Special Issue Fire Safety Journal on car park fire safety – Preface. Fire Saf J 57:2
- [6] Chow WK, Fung WY (1995) Survey on the indoor environment of enclosed car parks in Hong Kong. Tunn Undergr Space Technol 10:247-255
- [7] Chow WK (1996) Simulation of carbon monoxide level in enclosed car parks using an air flow network program. Tunn Undergr Space Technol 11:237-240
- [8] Chow WK, Wong LT, Fung WY (1996) Field study on the indoor thermal environment and carbon monoxide levels in a large underground car park. Tunn Undergr Space Technol 11:333-343
- [9] Chan MY, Burnett J, Chow WK (1998) Energy use for ventilation systems in underground car parks. Build Environ 33:303-314
- [10] Chow WK (1998). On safety systems for underground car parks. Tunn Undergr Space Technol 13:281-287
- [11] Viegas JC (2010) The use of impulse ventilation for smoke control in underground car parks. Tunn Undergr Space Technol 25:42-53
- [12] Zhang XG, Guo YC, Chan CK, Lin WY (2007) Numerical simulations on fire spread and smoke movement in an underground car park. Build Environ 42:3466-3475
- [13] Lin Z, Chow TT, Tsang CF, Fong KF, Chan LS, Shum WS (2008) Effect of ventilation system on smoke and fire spread in a public transport interchange. Fire Technol 44:463-479
- [14] Joyeux D (1997) Natural fires in closed car parks – Car fire tests. CTICM Report no. INC-96/294d-DJ/NB. Centre Technique Industriel Construction Métallique, Maizières-les-Metz, France

- [15] Schleich JB, Cajot L-G, Pierre M, Brasseur M, Franssen J-M, Kruppa J, Joyeux D, Twilt L, Van Oerle J, Aурtenetxe G (1999) Development of design rules for steel structures subjected to natural fires in closed car parks. Report EUR 18867. European Coal and Steel Community, Brussels, Belgium
- [16] Zhao B, Kruppa J (2004) Structural behaviour of an open car park under real fire scenarios. *Fire Mater* 28:269-280
- [17] Tilley N, Deckers X, Merci B (2012) CFD study of relation between ventilation velocity and smoke backlayering distance in large closed car parks. *Fire Saf J* 48:11-20
- [18] Horváth I, van Beeck J, Merci B (2013) Full-scale and reduced-scale tests on smoke movement in case of car park fire. *Fire Saf J* 57:35-43
- [19] Deckers X, Haga S, Sette B, Merci B (2013) Smoke control in case of fire in a large car park: Full-scale experiments. *Fire Saf J* 57:11-21
- [20] Deckers X, Haga S, Tilley N, Merci B (2013) Smoke control in case of fire in a large car park: CFD simulations of full-scale configurations. *Fire Saf J* 57:22-34
- [21] Fang C, Izzuddin BA, Obiala R, Elghazouli AY, Nethercot DA (2012) Robustness of multi-storey car parks under vehicle fire. *J Constr Steel Res* 75:72-84
- [22] Fang C, Izzuddin BA, Elghazouli AY, Nethercot DA (2013) Robustness of multi-storey car parks under localized fire – Towards practical design recommendations. *J Constr Steel Res* 90:193-208
- [23] Fang C, Izzuddin BA, Elghazouli AY, Nethercot DA (2013) Simplified energy-based robustness assessment for steel-composite car parks under vehicle fire. *Eng Struct* 49:719-732
- [24] Annerel E, Taerwe L, Merci B, Jansen D, Bamonte P, Felicetti R (2013) Thermo-mechanical analysis of an underground car park structure exposed to fire. *Fire Saf J* 57:96-106.
- [25] van der Heijden MGM, Loomans MGLC, Lemaire AD, Hensen JLM (2013) Fire safety assessment of semi-open car parks based on validated CFD simulations. *Build Simul* 6:385-394
- [26] Van den Schoor F, Middha P, Van den Bulck E (2013) Risk analysis of LPG (liquefied petroleum gas) vehicles in enclosed car parks. *Fire Saf J* 57:58-68
- [27] Merci B, Shipp M (2013) Smoke and heat control for fires in large car parks: Lessons learnt from research?. *Fire Saf J* 57:3-10
- [28] VdS (2015) Wassernebel-Sprinkleranlagen und Wassernebel-Löschanlagen (Hochdruck-Systeme), Planung und Einbau (Water mist-sprinkler systems and water-mist extinguishing systems – High-pressure systems, Planning and installation). VdS 3188. VdS Schadenverhütung, Cologne, Germany
- [29] European Committee for Standardization (2009) Fixed firefighting systems – Automatic sprinkler systems – Design, installation and maintenance. EN 12845:2004+A2:2009. CEN-CENELEC, Brussels, Belgium
- [30] Mangs J, Keski-Rahkonen O (1994) Characterization of the fire behaviour of a burning passenger car. Part I: Car Fire Experiments. *Fire Saf J* 23:17-35
- [31] Tohir MZM, Spearpoint M (2013) Distribution analysis of the fire severity characteristics of single passenger road vehicles using heat release rate data. *Fire Sci Rev* 2:5
- [32] Spearpoint MJ, Mohd Tohir MZ, Abu AK, Xie P (2015) Fire load energy densities for risk-based design of car parking buildings. *Case Stud Fire Saf* 3:44-50
- [33] Ren N, Blum A, Do C, Marshall AW (2009) Atomization and dispersion measurements in fire sprinkler sprays. *Atom Sprays* 19:1125-1136

- [34] Santangelo PE (2010) Characterization of high-pressure water-mist sprays: Experimental analysis of droplet size and dispersion. *Exp Therm Fluid Sci* 34:1353-1366
- [35] Santangelo PE (2012) Experiments and modeling of discharge characteristics in water-mist sprays generated by pressure-swirl atomizers. *J Therm Sci* 21:539-548
- [36] Santangelo PE, Tartarini P, Valdiserri P (2011) Experimental parametric analysis of water-mist sprays: An investigation on coalescence and initial dispersion. In: *Proceedings of ASME 2011 International Mechanical Engineering Congress and Exposition (IMECE 2011)*. Denver, CO, USA, vol 6, pp 1167-1174
- [37] Heskestad G (1972) Proposal for studying interaction of water sprays with plume in sprinkler optimization program. FMRC Interoffice Correspondence. FM Global, Norwood, MA, USA
- [38] Lefebvre AH (1989) *Atomization and Sprays*. Hemisphere, Washington, DC, USA
- [39] Lawson JR, Walton WD, Evans DD (1988) Measurement of droplet size in sprinkler sprays. NBSIR 88-3715. National Bureau of Standards, Gaithersburg, MD, USA
- [40] Santangelo PE, Tartarini P, Pulvirenti B, Valdiserri P, Marshall AW (2010) Fire suppression by water-mist sprays: Experimental and numerical analysis. In: *Proceedings of 14<sup>th</sup> International Heat Transfer Conference (IHTC-14)*. Washington, DC, USA, vol 5, pp 571-580
- [41] Santangelo PE, Tartarini P (2012) Full-scale experiments of fire suppression in high-hazard storages: A temperature-based analysis of water-mist systems. *Appl Therm Eng* 45-46:99-107
- [42] Giffen E, Muraszew A (1953) *Atomization of Liquid Fuels*. Chapman & Hall, London, UK
- [43] Rizk NK, Lefebvre AH (1985) Internal flow characteristics of simplex swirl atomizers. *J Propul Power* 1:193-199
- [44] Scheffey JL, Forssell EW, Childs JT (2013) Evaluation of water additives for fire control and vapor mitigation. Phase I Final Report. The Fire Protection Research Foundation, Quincy, MA, USA
- [45] Stroup DW, Madrzykowski D, Bishop MJ (1998) Chapter 2: Fire fighting properties. In: Madrzykowski D, Stroup DW (eds) *Demonstration of biodegradable, environmentally safe, non-toxic fire suppression liquids*. NISTIR 6191. National Institute of Standards and Technology, Gaithersburg, MD, USA
- [46] National Fire Protection Association (2015) NFPA 750 Standard on water mist fire protection systems. NFPA, Quincy, MA, USA
- [47] Ingason H, Wickström U (2007) Measuring incident radiant heat flux using the plate thermometer. *Fire Saf J* 42:161-166
- [48] Haremza C, Santiago A, Simões da Silva L (2013) Design of steel and composite open car parks. *Adv Steel Constr* 9:350-368
- [49] Yule HP (1969) Computation of experimental results in activation analysis. In: DeVoe JR, LaFleur PD (eds) *Modern trends in activation analysis*. National Bureau of Standards, Washington, DC, USA, vol 2, pp 1155-1204
- [50] Orlandini S, Moretti G, Corticelli MA, Santangelo PE, Capra A, Rivola R, Albertson JD (2012) Evaluation of flow direction methods against field observations of overland flow dispersion. *Water Resour Res* 48:W10523
- [51] Santangelo PE, Jacobs BC, Ren N, Sheffel JA, Corn ML, Marshall AW (2014) Suppression effectiveness of water-mist sprays on accelerated wood-crib fires. *Fire Saf J* 70:98-111

- [52] Shipp MP, Spearpoint MJ (1995) Measurements of the severity of fires involving private motor vehicles. *Fire Mater* 19:143-151
- [53] Li Y, Spearpoint M (2007) Analysis of vehicle fire statistics in New Zealand parking buildings. *Fire Technol* 43:93-106
- [54] Lönnermark A, Ingason H (2005) Fire spread in large industrial premises and warehouses. SP Report 2005:21. SP Swedish National Testing and Research Institute, Borås, Sweden
- [55] Heskestad G (2002) Scaling the interaction of water sprays and flames. *Fire Saf J* 37:535-548
- [56] Heskestad G (2003) Extinction of gas and liquid pool fires with water sprays. *Fire Saf J* 38:301-317
- [57] Liu Z, Kim AK, Su JZ (2001) Examination of performance of water mist fire suppression systems under ventilation conditions. *J Fire Prot Eng* 11:164-193

**Table 1** Experimental settings of the performed suppression tests

Test	Discharge density (L min <sup>-1</sup> m <sup>-2</sup> )	Nozzle type	K factor (L min <sup>-1</sup> bar <sup>-0.5</sup> )	Operative pressure (bar)	Area coverage (m <sup>2</sup> )	Configuration
C1SPK	6.5	Pendent sprinkler (with 68 °C bulb, standard response)	80	1	12	C1 (Fig. 1a)
C1WM1.5	1.5	Water mist (with 68 °C bulb, super fast response)	1.89	91	12	C1 (Fig. 1a)
C1WM2.0	2.0	Water mist (with bulb 68 °C, super fast response)	2.46	95	12	C1 (Fig. 1a)
C2SPK	6.5	Pendent sprinkler (with 68 °C bulb, standard response)	80	1	12	C2 (Fig. 1b)
C2WM1.5	1.5	Water mist (with 68 °C bulb, super fast response)	1.89	91	12	C2 (Fig. 1b)
C2WM2.0	2.0	Water mist (with 68 °C bulb, super fast response)	2.46	95	12	C2 (Fig. 1b)
C2WMA	1.5 (mixture, 3% additive)	Water mist (with 68 °C bulb, super fast response)	1.89	91	12	C2 (Fig. 1a)

**Table 2** Summary of damage evaluation in the tests on configuration C1

Test	Car	Damaged tires	Glasses	Spare tire	Exterior	Interior
C1SPK	Central	4 (50%)	0	not involved	severely burnt	evidence of materials loss
	Target 1	0	0	not involved	not involved	not involved
	Target 2	0	0	not involved	not involved	not involved
C1WM1.5	Central	1 (fully), 2 (50%)	1 (cracks)	not involved	severely burnt	evidence of materials loss
	Target 1	0	0	not involved	1 fender mildly burnt	not involved
	Target 2	0	0	not involved	lateral plastic parts mildly burnt	not involved
C1WM2.0	Central	2 (fully), 2 (50%)	0	not involved	severely burnt	unremarkably burnt
	Target 1	0	0	not involved	not involved	not involved
	Target 2	0	0	not involved	mildly blackened	not involved

**Table 3** Summary of damage evaluation in the tests on configuration C2

Test	Car	Damaged tires	Glasses	Spare tire	Exterior	Interior
C2SPK	Central	1 (fully), 3 (50%)	0	not involved	severely burnt	plastic materials burnt more than in test C1SPK
	Target 1	0	0	not involved	not involved	not involved
	Target 2	0	0	not involved	not involved	not involved
C2WM1.5	Central	1 (fully), 2 (50%)	0	not involved	severely burnt	unremarkably burnt
	Target 1	0	0	not involved	not involved	not involved
	Target 2	0	0	not involved	mildly blackened	not involved
C2WM2.0	Central	0	1 (cracks)	not involved	severely burnt	plastic materials remarkably burnt
	Target 1	0	0	not involved	not involved	not involved
	Target 2	0	0	not involved	not involved	not involved
C2WMA	Central	2 (50%)	4	burnt	very severely burnt	very severely burnt; fire intensely spread through the trunk
	Target 1	0	0	not involved	not involved	not involved
	Target 2	0	0	not involved	not involved	not involved

**Table 4** Nozzle activation times in the tests on configuration C1 (from heptane ignition)

Test	Activated nozzles	Activation time (s)
C1SPK	N1	290
	N2	290
	N5	589
C1WM1.5	N1	311
	N2	319
	N5	319
	N6	346
	N7	1156
C1WM2.0	N1	173
	N5	173
	N6	243
	N7	243



**Table 5** Nozzle activation times in the tests on configuration C2 (from heptane ignition)

Test	Activated nozzles	Activation time (s)
C2SPK	N8	182
	N9	212
	N10	220
	N11	241
C2WM1.5	N8	136
	N9	136
	N10	136
	N11	317
C2WM2.0	N8	202
	N9	221
	N10	225
	N11	231
C2WMA	N8	82
	N9	82
	N10	82
	N11	130

## Figure captions

**Fig. 1** Technical sketch of the experimental facility (view from above): a) first configuration (C1), ignition source axially under a nozzle; b) second configuration (C2), ignition source in the middle of the area covered by 4 nozzles; F: flow meter, N: nozzle, P: pressure gauge, PT: plate thermometer, TC: thermocouple

**Fig. 2** Sketch of the front view of the experimental facility (not to scale), with sizes of the tilt-out opening and of the average gap between the secondary ceiling (test chamber) and the walls

**Fig. 3** Car arrangement within the test chamber; nozzles and piping are also visible in this photo, below the ceiling; plate thermometers are also visible in front of each car

**Fig. 4** Photos and technical sketches of plane sections: a) sprinkler nozzle; b) water-mist nozzle (detail of a generic injector)

**Fig. 5** Photos of the exterior of the central car used in test C1SPK: a) before and b) after testing

**Fig. 6** Photos of the interior of the central car used in test C1SPK: a) before and b) after testing

**Fig. 7** Photos of the interior of the central car used in test C1WM1.5: a) before and b) after testing

**Fig. 8** Photos of the exterior of a) Target 1 car used in test C1WM1.5, b) Target 2 car used in test C1WM1.5 and c) Target 2 car used in test C1WM2.0 after testing

**Fig. 9** Photo of the interior of the central car used in test C2SPK after testing

**Fig. 10** Photos of the interior of the central car used in test C2WM2.0: a) before and b) after testing

**Fig. 11** Photos of the exterior of the central car used in test C2WMA after testing

**Fig. 12** Photos of the interior of the central car used in test C2WMA: a) before and b) after testing

**Fig. 13** Temperature trends for configuration C1. a) readings from thermocouple TC5: — C1SPK, — C1WM1.5, — C1WM2.0; b) peak temperature  $\Delta T_{peak}$  (- - C1SPK, - - C1WM1.5, - - C1WM2.0) and average temperature  $\Delta T_{ave}$  (··· C1SPK, ··· C1WM1.5, ··· C1WM2.0); 0: first nozzle activated, 1: last nozzle activated in test C1SPK, 2: last nozzle activated in test C1WM1.5, 3: last nozzle activated in test C1WM2.0

**Fig. 14** Temperature time trends for configuration C2. a) readings from thermocouple TC5: — C2SPK, — C2WM1.5, — C2WM2.0, — C2WMA; b) peak temperature  $\Delta T_{peak}$  (- -

C2SPK, - - C2WM1.5, - - C2WM2.0, - - C2WMA) and average temperature  $\Delta T_{ave}$  ( $\cdots$  C2SPK,  $\cdots$  C2WM1.5,  $\cdots$  C2WM2.0,  $\cdots$  C2WMA); 0: first nozzle activated, 1: last nozzle activated in test C2SPK, 2: last nozzle activated in test C2WM1.5, 3: last nozzle activated in test C2WM2.0, 4: last nozzle activated in test C2WMA

**Fig. 15** Trends of first derivative of average temperature  $\Delta T_{ave}$ : a) test C1SPK; b) test C1WM1.5; c) test C1WM2.0; d) test C2SPK; e) test C2WM1.5; f) test C2WM2.0; g) test C2WMA; F: first nozzle activated, L: last nozzle activated

**Fig. 16** Summary of relevant, single-value expressions of temperature maxima for all the tests performed against both the explored configurations: ■  $\Delta T_{peak}$ , ■  $\Delta T_{peak,ave}$  – Eq. (4), ■  $\Delta T_{max,ave}$  – Eq. (6)

**Fig. 17** Trend of incident radiant heat flux onto plate thermometer PT1 from ignition through activation of the first nozzle: — C1SPK, — C1WM1.5, — C1WM2.0, - - C2SPK, - - C2WM1.5, - - C2WM2.0, - - C2WMA

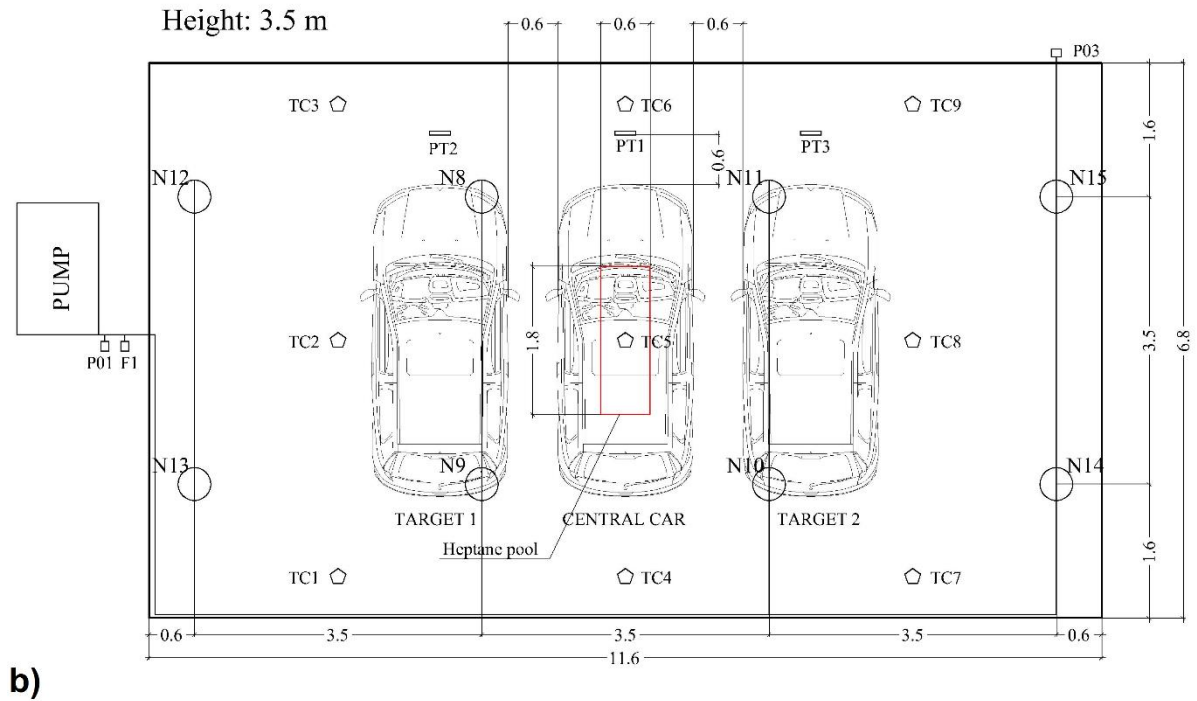
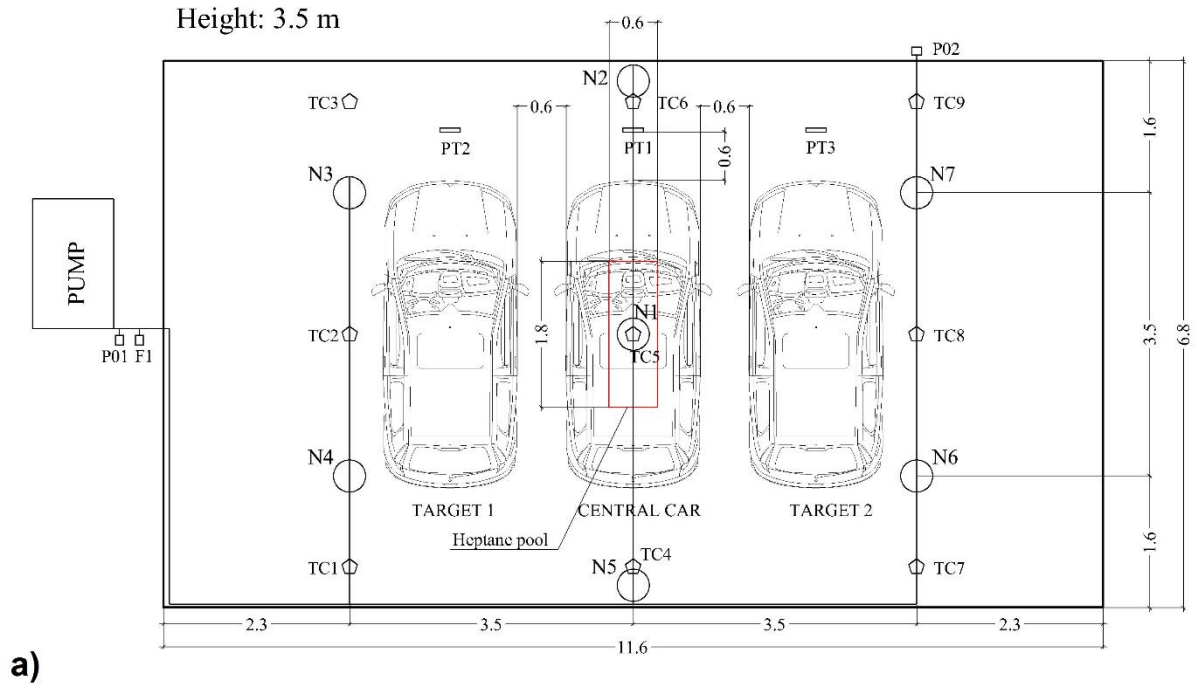


**Fig. 1** Technical sketch of the experimental facility (view from above): a) first configuration (C1), ignition source axially under a nozzle; b) second configuration (C2), ignition source in the middle of the area covered by 4 nozzles; F: flow meter, N: nozzle, P: pressure gauge, PT: plate thermometer, TC: thermocouple

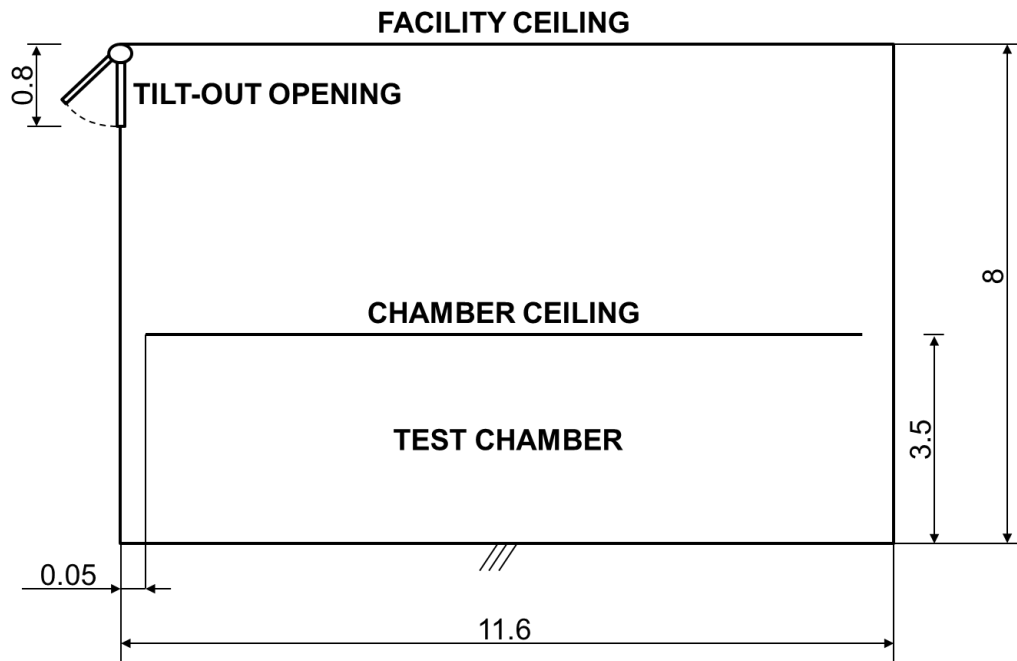


**Fig. 2** Sketch of the front view of the experimental facility (not to scale), with sizes of the tilt-out opening and of the average gap between the secondary ceiling (test chamber) and the walls



**Fig. 3** Car arrangement within the test chamber; nozzles and piping are also visible in this photo, below the ceiling; plate thermometers are also visible in front of each car

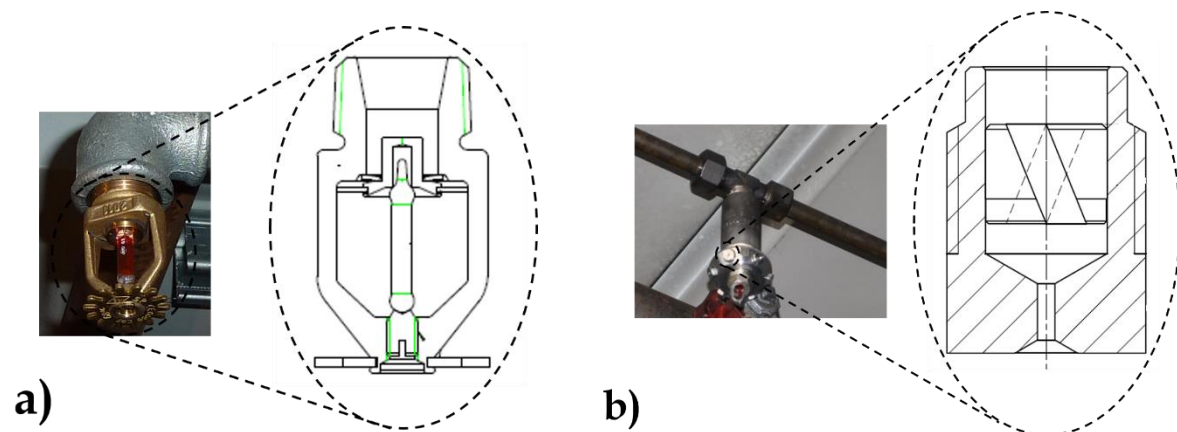


**Fig. 4** Photos and technical sketches of plane sections: a) sprinkler nozzle; b) water-mist nozzle (detail of a generic injector)



**Fig. 5** Photos of the exterior of the central car used in test C1SPK: a) before and b) after testing





a)



b)

**Fig. 6** Photos of the interior of the central car used in test C1SPK: a) before and b) after testing

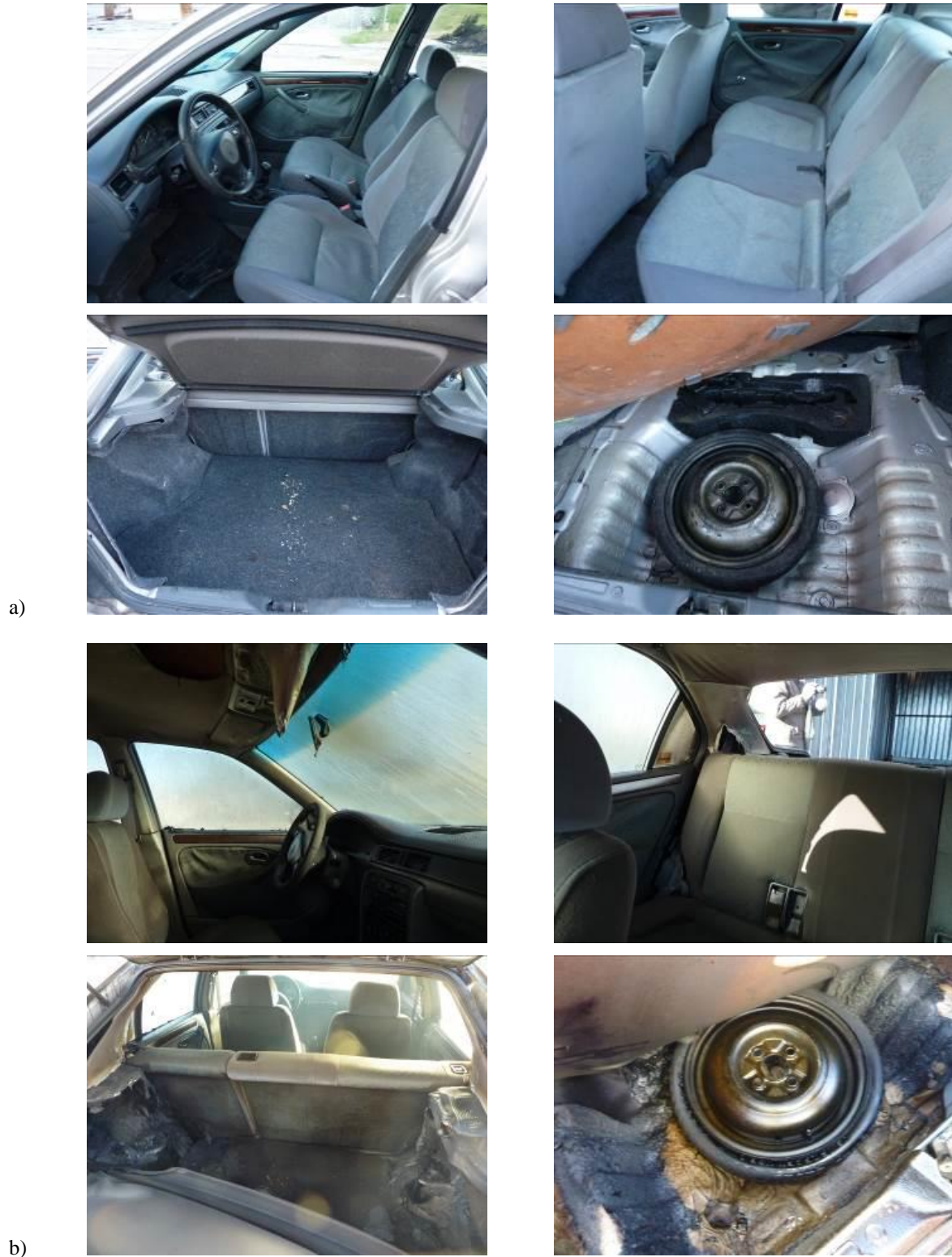


**Fig. 7** Photos of the interior of the central car used in test C1WM1.5: a) before and b) after testing

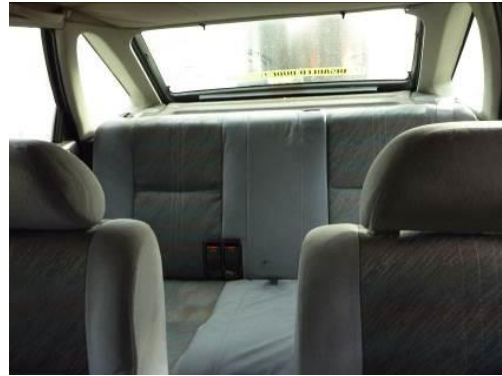




**Fig. 8** Photos of the exterior of a) Target 1 car used in test C1WM1.5, b) Target 2 car used in test C1WM1.5 and c) Target 2 car used in test C1WM2.0 after testing



**Fig. 9** Photo of the interior of the central car used in test C2SPK after testing



a)



b)

**Fig. 10** Photos of the interior of the central car used in test C2WM2.0: a) before and b) after testing



**Fig. 11** Photos of the exterior of the central car used in test C2WMA after testing





**Fig. 12** Photos of the interior of the central car used in test C2WMA: a) before and b) after testing

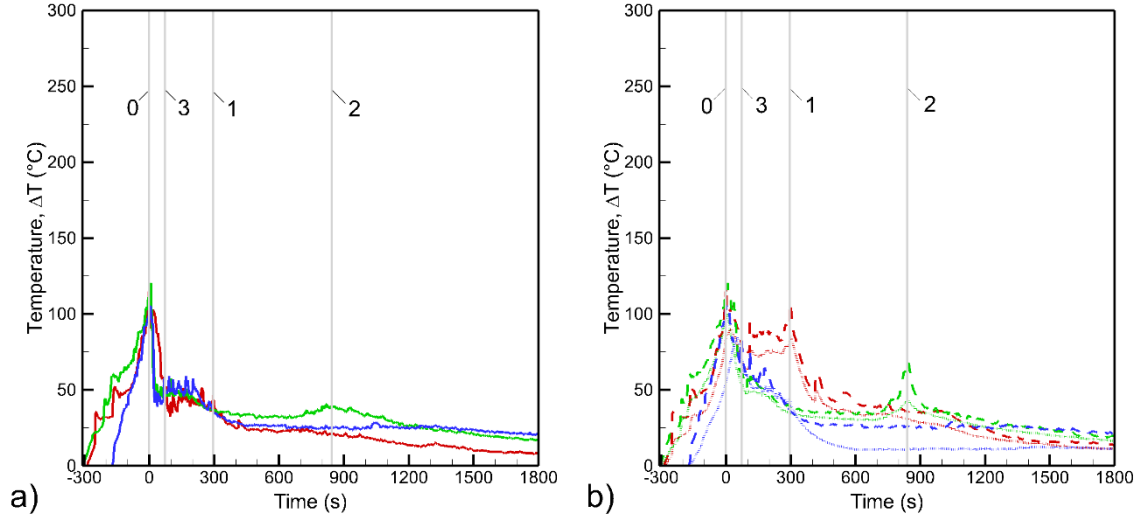


**Fig. 13** Temperature trends for configuration C1. a) readings from thermocouple TC5: — C1SPK, — C1WM1.5, — C1WM2.0; b) peak temperature  $\Delta T_{peak}$  (--- C1SPK, --- C1WM1.5, --- C1WM2.0) and average temperature  $\Delta T_{ave}$  (···· C1SPK, ···· C1WM1.5, ···· C1WM2.0); 0: first nozzle activated, 1: last nozzle activated in test C1SPK, 2: last nozzle activated in test C1WM1.5, 3: last nozzle activated in test C1WM2.0

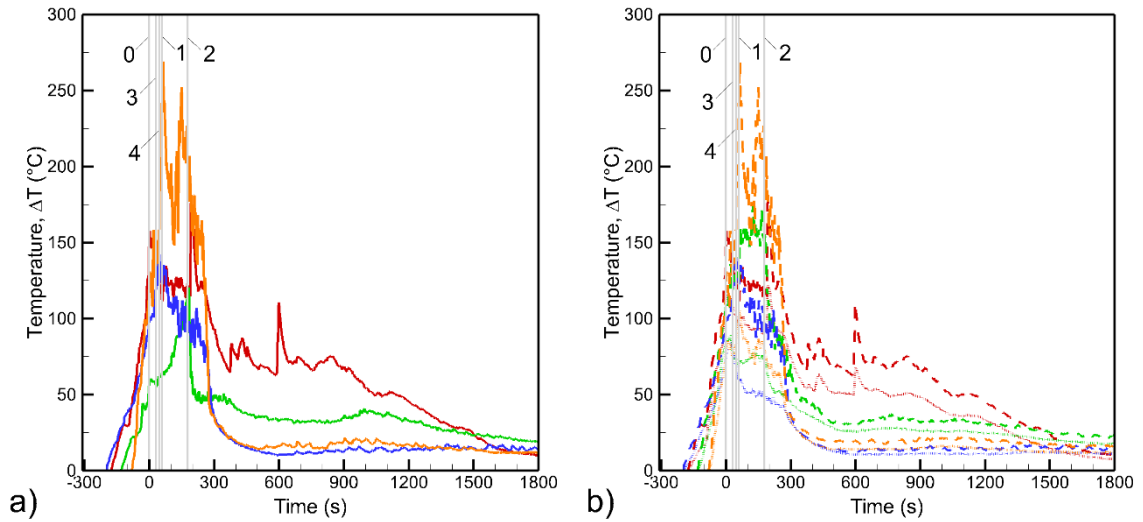


**Fig. 14** Temperature time trends for configuration C2. a) readings from thermocouple TC5: — C2SPK, — C2WM1.5, — C2WM2.0, — C2WMA; b) peak temperature  $\Delta T_{peak}$  (--- C2SPK, --- C2WM1.5, --- C2WM2.0, --- C2WMA) and average temperature  $\Delta T_{ave}$  (···· C2SPK, ···· C2WM1.5, ···· C2WM2.0, ···· C2WMA); 0: first nozzle activated, 1: last nozzle activated in test C2SPK, 2: last nozzle activated in test C2WM1.5, 3: last nozzle activated in test C2WM2.0, 4: last nozzle activated in test C2WMA

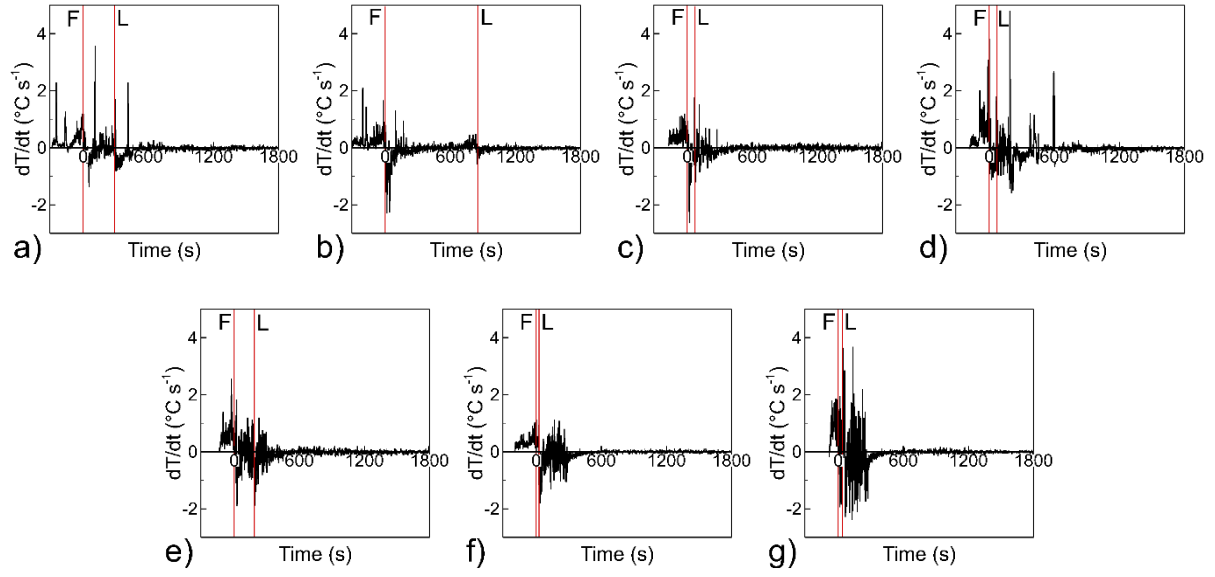


**Fig. 15** Trends of first derivative of average temperature  $\Delta T_{ave}$ : a) test C1SPK; b) test C1WM1.5; c) test C1WM2.0; d) test C2SPK; e) test C2WM1.5; f) test C2WM2.0; g) test C2WMA; F: first nozzle activated, L: last nozzle activated

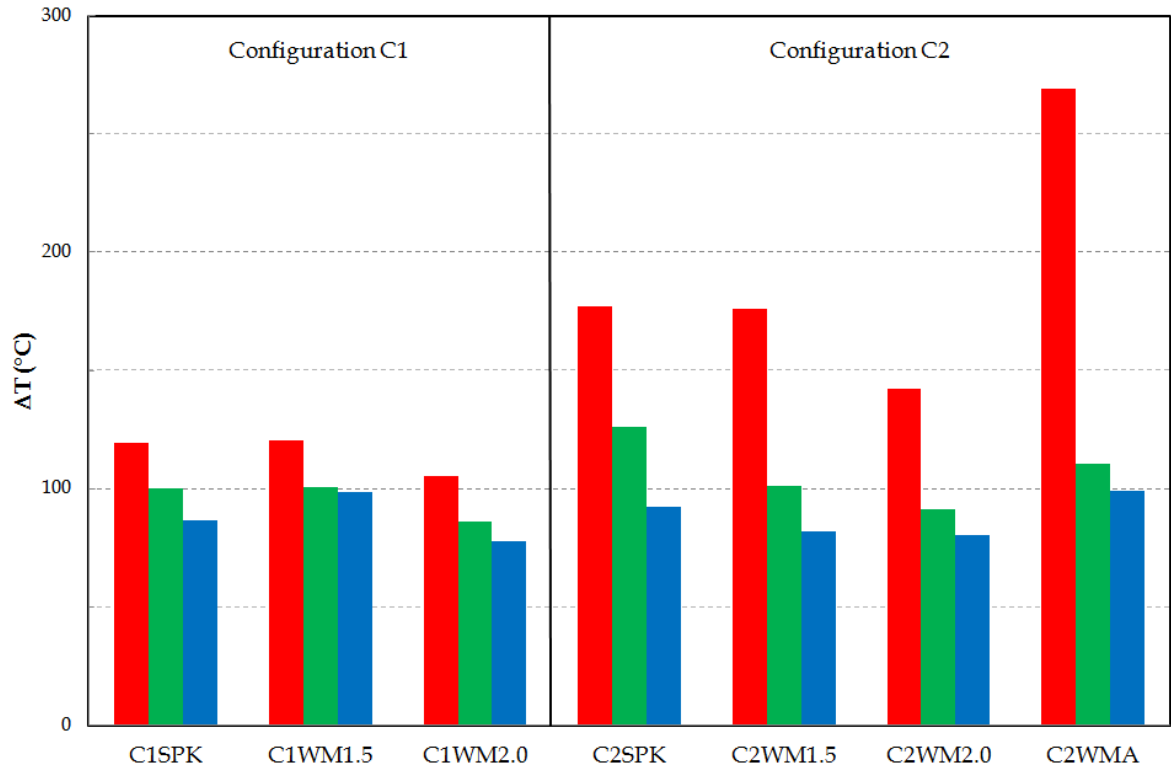


**Fig. 16** Summary of relevant, single-value expressions of temperature maxima for all the tests performed against both the explored configurations: ■  $\Delta T_{peak}$ , ■  $\Delta T_{peak,ave}$  - Eq. (4), ■  $\Delta T_{max,ave}$  - Eq. (6)

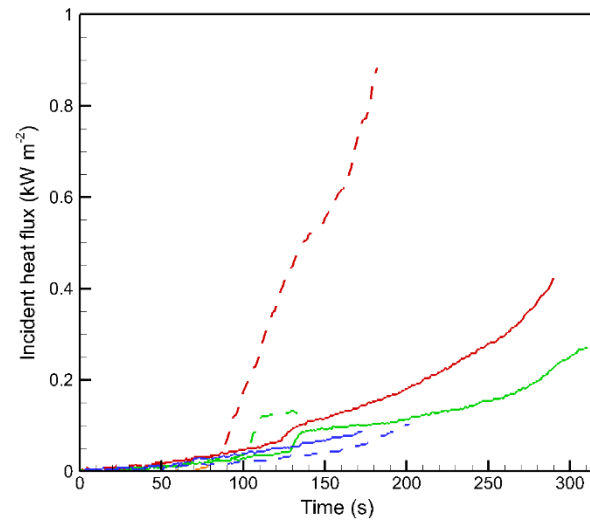


**Fig. 17** Trend of incident radiant heat flux onto plate thermometer PT1 from ignition through activation of the first nozzle: — C1SPK, — C1WM1.5, — C1WM2.0, - - C2SPK, - - C2WM1.5, - - C2WM2.0, - - C2WMA